JOURNAL OF MATERIALS SCIENCE 27 (1992) 13–23

Stress–strain behaviour at finite strains for various strain paths in polyethylene

MASAYOSHI KITAGAWA, TETSUYUKI ONODA, KAZUNOBU MIZUTANI
Department of Mechanical Engineering, Faculty of Technology, Kanazawa University, Kanazawa, Japan

In order to provide new experimental facts required for constructing a non-linear constitutive equation for crystalline polymers, some tests were conducted by the use of polyethylene (PE) under various strain histories such as tension, torsion, tension–torsion proportional strain path, tension–torsion cruciform strain path, tension–torsion circular strain path, and various cyclic loadings. It is shown that (i) since the stress–strain behaviour for PE is not very sensitive to hydrostatic pressure, the equivalent stress and strain of von Mises type are useful for its description; (ii) the stress range at a constant strain amplitude at partly reversed cyclic loading tends to increase with an increase in the number of cycles, but the stress amplitude at fully reversed cyclic loading is nearly independent of the number of cycles; (iii) the degree of cyclic softening or hardening is relatively small compared with that of polypropylene; and (iv) under the conditions tested here, the effect of strain history on the stress–strain response is hardly observed for PE.

1. Introduction

Although much effort [1, 2] has been made to introduce a non-linearity in the linear theory of viscoelasticity, non-linear behaviour at finite strain is less well understood because of the many complexities peculiar to polymer solids. Many interesting and excellent experimental data on yielding and fracture for both crystalline and amorphous polymer solids have been published [3–7] and some qualitative explanations of the plastic deformation have been proposed [8–10]. However, they seem to be far from a complete description of the plastic deformation behaviour. Even the definition of yielding still seems vague. Furthermore, the very relationship between stress and strain in the finite strain range was little investigated, and therefore less well understood.

For metals, on the physical basis of both plastic potential theory and dislocation theory, the stress–strain behaviour under various strain paths has been described quantitatively and qualitatively with success. For polymers, the constitutive law proposed for metals cannot be applied without modification due to the difference of the deformation mechanism between polymer and metal.

Recently, Parks and Boyce [11] proposed a constitutive model for amorphous polymers and applied it successfully to the hydrostatic extrusion of polymethylmethacrylate. Vest *et al.* [12] proposed a mechanical model which consists of four elements and described the stress–strain behaviour at constant strain-rate tension. Previous papers [13–16] have shown that a constitutive equation based on an overstress model proposed by Krempl [17, 18] was appropriate for the description of the stress–strain behaviour for polyethylene and polypropylene.

However, if the current strain is less than the maximum strain, the stress–strain behaviour is strongly affected by the strain history and these theories are not a good approximation of the stress–strain behaviour for polymers. Unfortunately, an effective means for the description of a constitutive law has not been found to date.

In order to construct a constitutive law for polymers, wide knowledge will be needed concerning the stress–strain responses at finite strains. The goals of this paper are (i) to provide some experimental data under various strain histories and (ii) to point out some important facts required for the construction of the constitutive model. For these purposes, the stress–strain curves were investigated under various complex strain histories using a type of crystalline polymer, polyethylene. For the results of tests under monotonous strain paths such as strain-rate dependence, abrupt change in strain rate and stress relaxation, earlier publications [13, 14] should be consulted.

2. Experimental procedure

2.1. Material

The material used was extruded rods of commercial polyethylene (PE). They were annealed for 2 h at 70 °C. As described elsewhere [14], the degree of anisotropy for the annealed rods was found to be very small. Solid cylindrical specimens with diameter 12 mm and gauge length 20 mm, and hollow cylindrical specimens with outer and inner diameters 16 and

0022–2461/92 $03.00 + .12

12 mm, respectively, and gauge length 21 mm, were machined from the rods. After machining, the specimens were again annealed for 2 h at 70 °C. The former specimens were used for tension and compression, and the latter ones were used for combined tension–torsion. Besides these specimens, small hollow cylinders with outer and inner diameters 8 and 6 mm, respectively, and gauge length 12 mm were machined and were used for observing pressure-dependent behaviour.

The stress was calculated based on the assumption that the material is incompressible and the cylinder is thin-walled. This assumption for the polymer used was supported by previous tests [19]. For combined tension–torsion, the tensile stress σ and the shear stress τ were calculated from

$$\sigma = \frac{F(1 + \varepsilon_n)}{A_0} \quad (1)$$

$$\tau = \frac{T(1 + \varepsilon_n)^{3/2}}{(r_0 A_0)} \quad (2)$$

and the tensile strain ε and shear strain γ were computed from

$$\varepsilon = \ln(1 + \varepsilon_n) \quad (3)$$

$$\gamma = \frac{r_0}{l_0}\theta(1 + \varepsilon_n)^{-3/2} \quad (4)$$

where $\varepsilon_n = (l - l_0)/l_0$ is the nominal strain, l and l_0 are the current and the original gauge length, F is the applied force, T is the torque, r_0 is the original mean radius of the hollow cylinder, A_0 is the original cross-sectional area and θ is the twist angle over the gauge length.

An equivalent tensile strain $\varepsilon_{eq.}$, its rate $\dot{\varepsilon}_{eq.}$ and an equivalent tensile stress $\sigma_{eq.}$ defined by

$$\varepsilon_{eq.} = \left(\varepsilon^2 + \frac{\gamma^2}{3}\right)^{1/2} \quad (5)$$

$$\dot{\varepsilon}_{eq.} = \left(\dot{\varepsilon}^2 + \frac{\dot{\gamma}^2}{3}\right)^{1/2} \quad (6)$$

$$\sigma_{eq.} = (\sigma^2 + 3\tau^2)^{1/2} \quad (7)$$

were used for the data arrangement. $\dot{\varepsilon}$ and $\dot{\gamma}$ are the axial and shear strain rates, respectively.

2.2. Strain paths

In order to investigate the effect of the strain history on the stress–strain curve, various strain paths schematically illustrated in Table I were applied to the specimens and the stress responses were measured. For the sake of convenience, the axial strain rate was controlled by use of the nominal strain rate $\dot{\varepsilon}_n = \dot{l}/l_0$ in the present tests. The strain rate described below then represents the nominal strain rate. From these tests the following were investigated; (i) the validity of the relationship between $\sigma_{eq.}$ and $\varepsilon_{eq.}$, (ii) the effect of strain history on the stress–strain behaviour, and (iii) the stress responses to some complex strain paths. These experimental data will be useful for considering the construction of the non-linear constitutive equation at finite strains for polymer solids.

For these tests, a hydraulic servo-controlled tension–compression testing machine (dynamic servo; Saginomiya Co., Japan), a home-made combined tension–torsion testing machine and a home-made torsion testing machine equipped with a high-pressure vessel were used. All the experiments were conducted at 25 °C.

3. Results and discussion

3.1. Monotonous tension and torsion

Fig. 1 shows the $\sigma_{eq.}$–$\varepsilon_{eq.}$ curves for compression and torsion executed at $\dot{\varepsilon}_{eq.} = 1.4 \times 10^{-3}\,s^{-1}$. For PE, the transition from elastic to plastic behaviour is gradual without a sharp yield drop, and slight work-hardening is observed. It may be difficult to define yielding strictly. The experimental distinction between elastic and plastic strain may therefore seem impossible. Data for both compression and torsion may be recognized to follow the same curve within experimental error. This demonstrates that the stress–strain behaviour is hardly affected by the hydrostatic stress component. According to the experimental data obtained under high hydrostatic pressures, the flow stress of PE is relatively insensitive to hydrostatic pressure compared with polypropylene [20]. Hence, the equivalent stress and equivalent strain defined in Equations 5 and 7 will be useful for PE at atmospheric pressure.

A combined tension–torsion test was executed to ensure the validity of the relationship between $\sigma_{eq.}$ and $\varepsilon_{eq.}$. The experimental data, obtained at nearly the same strain rate as adopted in the previous section, are also shown in Fig. 1. The data for the two tests are found to nearly fall on the uniaxial test data mentioned above. Hence, it is concluded that the use of $\sigma_{eq.}$ and $\varepsilon_{eq.}$ defined in Equations 5 and 7 is appropriate to the treatment of the stress–strain behaviour of PE.

Fig. 2 represents the torsional creep curves at various stress levels. It is shown that with an increase in testing time, the creep strain increases, but the strain rate decreases since the curves are convex upwards. Even at relatively high stresses, the shape of the curves is similar to that at low stresses. On the other hand, for polypropylene (PP) subjected to high stresses, three stages (primary, secondary and tertiary creep) can be observed [16]. At the tertiary stage, the creep strain increases with increasing time in an accelerating fashion and, therefore, the creep curve become convex downwards. This difference of creep behaviour between PE and PP may be important for discussing the constitutive equation.

3.2. Strain reversal

Fig. 3 denotes the stress–strain behaviour after strain reversal. After solid cylindrical specimens were compressed at a constant strain rate of $\dot{\varepsilon}_0 = 9 \times 10^{-4}\,s^{-1}$ up to $\varepsilon = -0.2$, unloading was executed at various strain rates from $\dot{\varepsilon}_0/50$ to $100\dot{\varepsilon}_0$. It is interesting to note that (i) the shape of the curves after strain reversal

TABLE I Schematic illustration of strain paths tested

Name	Waveform	Strain trajectory	
(a) Tension-compression or torsion	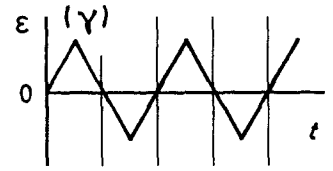	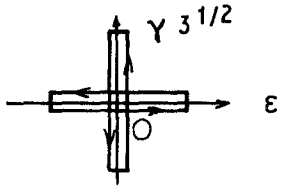	$\varepsilon = \lvert \dot{\varepsilon} \rvert t$ or $\gamma = \lvert \dot{\gamma} \rvert t$
(b) Proportion	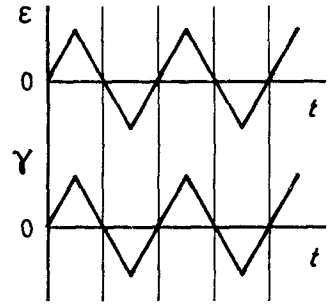	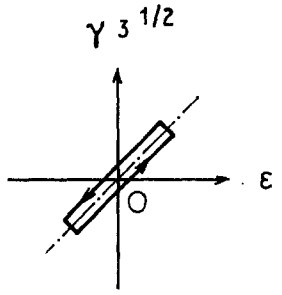	$\varepsilon = \lvert \dot{\varepsilon} \rvert t$ and $\gamma = \lvert \dot{\gamma} \rvert t$
(c) Cruciform	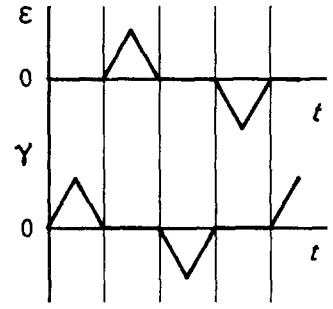	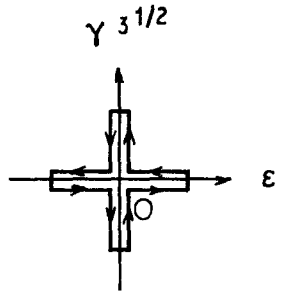	$\varepsilon = \lvert \dot{\varepsilon} \rvert t$ or $\gamma = \lvert \dot{\gamma} \rvert t$
(d) Circular	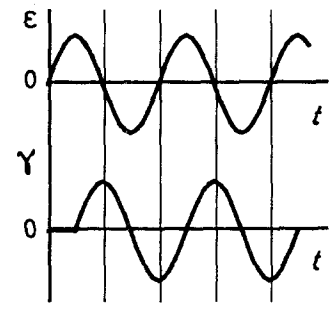	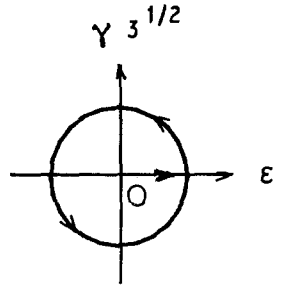	$\varepsilon = a \sin \omega t$ $\gamma = 3^{1/2} a \cos \omega t$ $a\,\omega = \text{const.}$

is dependent on strain rate, and (ii) the higher the strain rate, the steeper the tangential slope just after strain reversal.

Judging from the shape of the stress–strain curves, to identify where yielding occurs seems to be more difficult after strain reversal than before strain reversal. Even the definition of yielding may become vague, especially after strain reversal. The residual strain at the point where the curve crosses the horizontal axis is found to be strongly dependent on the strain rate at unloading. For example, when unloading is performed at the strain rate of $\dot{\varepsilon}_0/50$, the residual strain is only half of the initially applied strain. It is indicated that the higher the reversal strain rate, the larger the residual strain. If the specimen is left in a stress-free state as it is, the residual strain recovers continuously with an increase in elapsed time and finally reaches a stable value. The permanent strain which remains after the lapse of more than one month becomes about 1/3 of the applied strain. Furthermore, the permanent strain is dependent on the unloading strain path. The details were reported elsewhere [13].

The tangential slope at a strain rate of $\dot{\varepsilon}_0/50$ becomes 1000 times larger than the initial modulus, probably due to stress relaxation. Hence, the assumption that the elastic modulus is constant in all strain ranges may be meaningless for PE.

These facts may show that an exact distinction between elastic and plastic strain is difficult. Hence, it may be inadequate to try to construct a constitutive law of polymers by means of the plastic potential theory which has been successfully applied for steels.

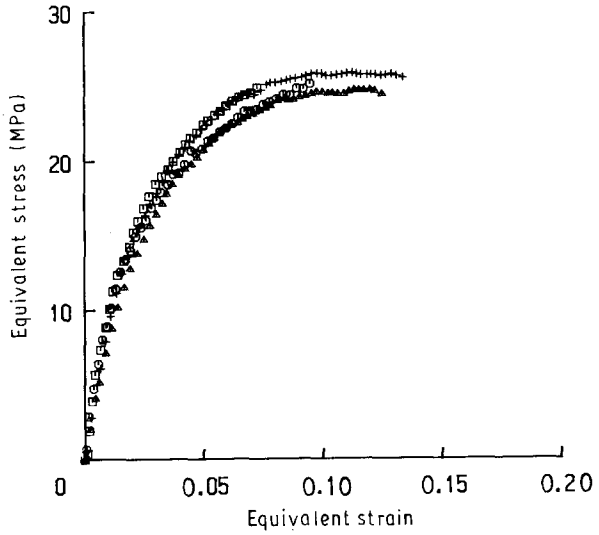

Figure 1 Equivalent stress–equivalent strain curves at an equivalent strain rate of about $\dot{\varepsilon}_{eq.} = 1.4 \times 10^{-3} s^{-1}$ for (○) compression, (□) torsion and (△, +) combined tension–torsion; ratio of axial strain rate to shear strain rate $R = 0.58$.

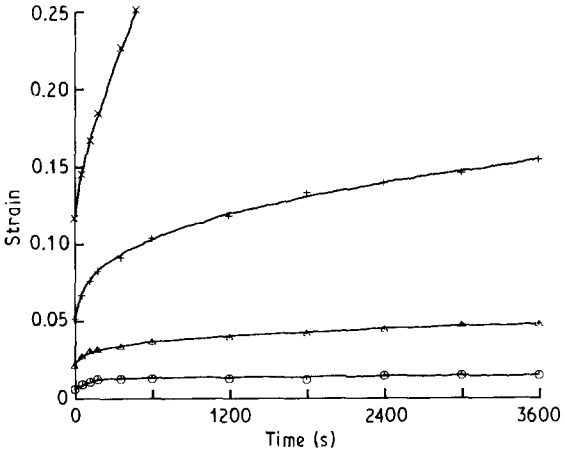

Figure 2 Creep curves for torsion at shear stress τ = (○) 0.3, (△) 0.6, (+) 0.9 and (×) 1.2 kgf mm^{-2}. Creep test started after torsion was conducted to a predetermined stress level at a strain rate of $1.2 \times 10^{-3} s^{-1}$.

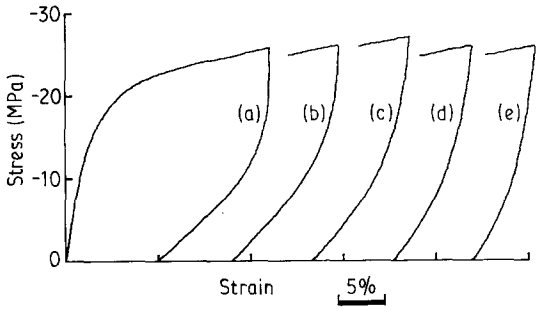

Figure 3 Stress–strain curves after strain reversal. After compression was executed to an axial strain of -0.2 at a strain rate of $\dot{\varepsilon} = -9 \times 10^{-4} s^{-1}$, unloading was done at strain rate (a) (1/50) $\dot{\varepsilon}$, (b) (1/10) $\dot{\varepsilon}$, (c) $\dot{\varepsilon}$, (d) $10\dot{\varepsilon}$ and (e) $100\dot{\varepsilon}$. The curves are shifted arbitrarily along the horizontal axis.

The relaxation behaviour after strain reversal was investigated. The specimen was compressed up to a reversal point of $\varepsilon = -0.2$ at a strain rate of $9 \times 10^{-4} s^{-1}$, subsequent unloading was executed at the same strain rate up to a predetermined strain, and the strain was kept constant (the relaxation started). The variation of stress as a function of elapsed time is shown in Fig. 4 where the result for a relaxation test without strain reversal is also represented. In the case without strain reversal, the absolute value of stress continues to decrease with increasing time and tends to gradually approach a stable value. In contrast, when the magnitude of strain reversal, $\Delta\varepsilon$, is large, it continues to increase with increasing time until it reaches an asymptotic value. In the case where $\Delta\varepsilon$ is small, a curious behaviour is observed in that the absolute value of stress at first increases for a while and then decreases continuously with time until it approaches a stable value asymptotically. This anomalous behaviour has not been reported to date. Let us now call this phenomenon the anomalous behaviour of stress relaxation. This anomalous behaviour can probably be attributed to the strongly time-sensitive characteristics of polymers. The temperature alteration during the test may not be a principal reason for this behaviour, since it is only less than 1 °C and hence is too small to cause the anomalous stress variation through thermal expansion. Unfortunately, the reason why this is caused is unclear. An anomalous behaviour of creep was also observed, in that when a creep test was executed after strain reversal, the creep strain at first decreased for a while and subsequently increased with time. This creep behaviour will be reported elsewhere.

In addition, after the applied strain was reversed up to a constant strain of 0.19 at various strain rates from the strain reversal point of $\varepsilon = -0.2$, the relaxation response was measured. Fig. 5 shows the stress variation with elapsed time. Except that the smaller the

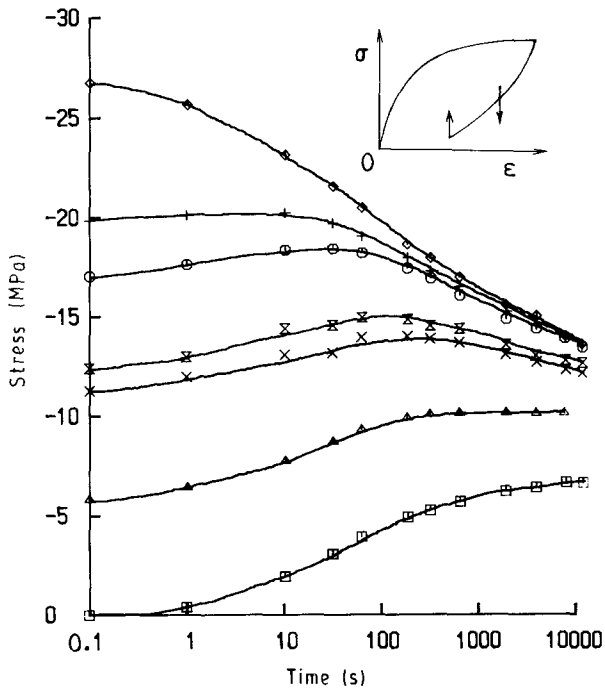

Figure 4 Variation of relaxation stress with elapsed time. After compression up to an axial strain of -0.2 at a strain rate of $-9 \times 10^{-4} s^{-1}$, unloading was performed at the same strain rate magnitude to predetermined strain levels (◇) -0.2, (+) -0.195, (○) -0.19, (⧖) -0.18, (×) -0.176, (△) -0.15, and (□) -0.115 and relaxation then started.

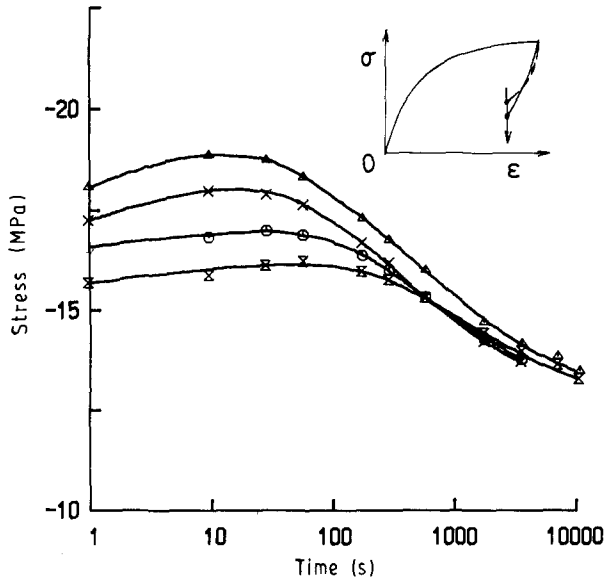

Figure 5 Variation of relaxation stress with time. After compression up to axial strain of -0.2 at a strain rate of $\dot{\varepsilon} = -9 \times 10^{-4} s^{-1}$, unloading was done to a strain of -0.19 at different strain rates (△) $10\dot{\varepsilon}$, (×) $\dot{\varepsilon}$, (○) $(1/3)\dot{\varepsilon}$ and (⧖) $(1/10)\ \dot{\varepsilon}$ and, relaxation then started.

strain rate after strain reversal, the higher the initial stress at $\varepsilon = -0.19$, the shape of the relaxation curve seems independent of the strain rate preceding the relaxation test. The stress magnitude at first increases and successively decreases in a gradual manner with elapsed time. After the elapse of a long period, the stress seems to approach a constant value which is independent of the strain rate preceding the relaxation test.

3.3. Cyclic loading

Fig. 6a and b show the tension–compression and torsional hysteresis loops, respectively, for fully reversed cyclic loading at a constant equivalent strain amplitude of 0.05 in a sinusoidal waveform. Comparison between them shows that the two hysteresis loops described in a $\sigma_{eq.}$–$\varepsilon_{eq.}$ diagram are nearly coincident, and therefore a von Mises type of equivalent stress is useful for cyclic loading as well as for monotonous loading. It is important to note that cyclic hardening or softening is hardly observed. These features were also found at another strain amplitude.

The effect of hydrostatic pressure on the cyclic stress–strain behaviour was investigated under torsion in the pressure range 1 to 1800 kgf cm^{-2} [20]. According to the results, (i) the higher the hydrostatic pressure, the larger the flow stress, (ii) the flow stress for PE is more insensitive to hydrostatic pressure than that for PP, and (iii) the shape of the hysteresis loop seems to be independent of hydrostatic pressure. In the pressure range tested here, the experimental trends obtained at atmospheric pressure hold true at high pressure. The reverse is also true [20].

Next, the results for partly reversed cyclic loading are discussed. To facilitate the interpretation of the results for partly reversed cyclic loading, a schematic illustration of hysteresis loops and strain histories is given in Fig. 7. After constant strain-rate torsion up to $\gamma_1 = \gamma_{max.}$, a partly reversed cyclic loading was executed for several cycles in the strain range $\gamma_1 = \gamma_{max.}$ $\gamma_1 = \gamma_{max.}$ to $\gamma_2 = \gamma_{min.}$ (Step I). Subsequently torsion was performed up to $\gamma_4 = -\gamma_{max}$ and then a new cyclic loading test in the strain range $\gamma_4 = -\gamma_{max.}$ to $\gamma_3 = -\gamma_{min.}$ was performed (Step II). Finally, a fully reversed cyclic loading in the strain range $\gamma_4 = -\gamma_{max.}$ to $\gamma_1 = \gamma_{max.}$ was applied in one cycle (Step III).

Fig. 8 shows an example of the experimental hysteresis loops at $\gamma_{max.} = 0.13$ and $\gamma_{min.1} = 0$. We first consider the stress–strain curves at Step I. The stress at the maximum strain $\gamma_{max.}$ is nearly constant independent of the number of cycles, but the stress at the minimum strain γ_2 decreases with an increase in the number of cycles and gradually approaches a stable value. In other words, for a partly reversed loading,

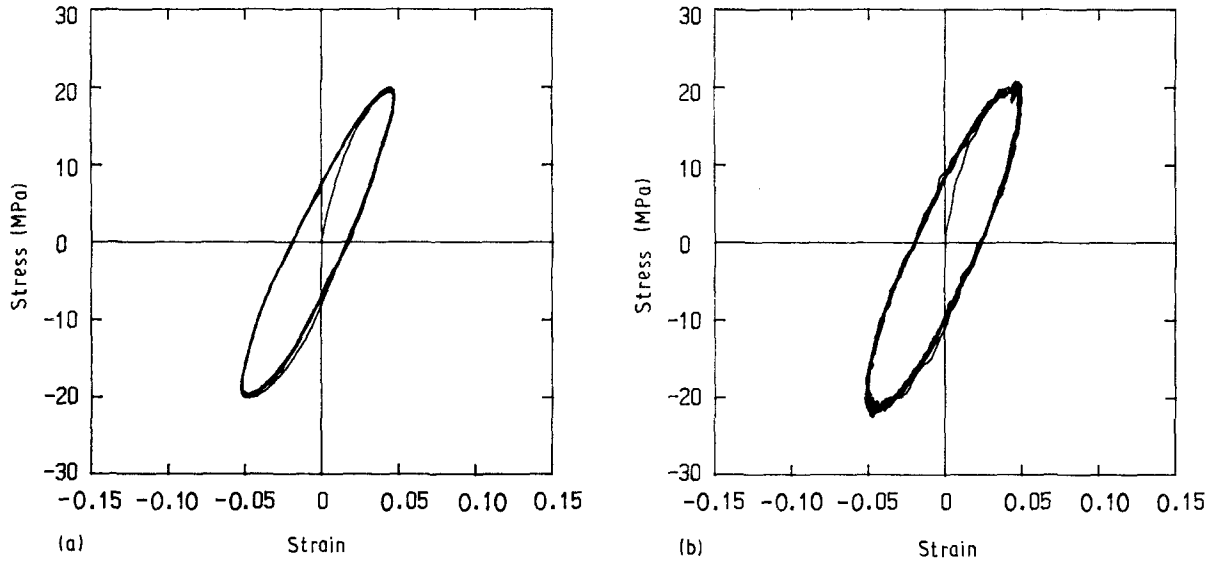

Figure 6 (a) Tension–compression and (b) torsional hysteresis loops at an equivalent strain amplitude of 0.05 in a sinusoidal waveform with frequency 1/300 Hz.

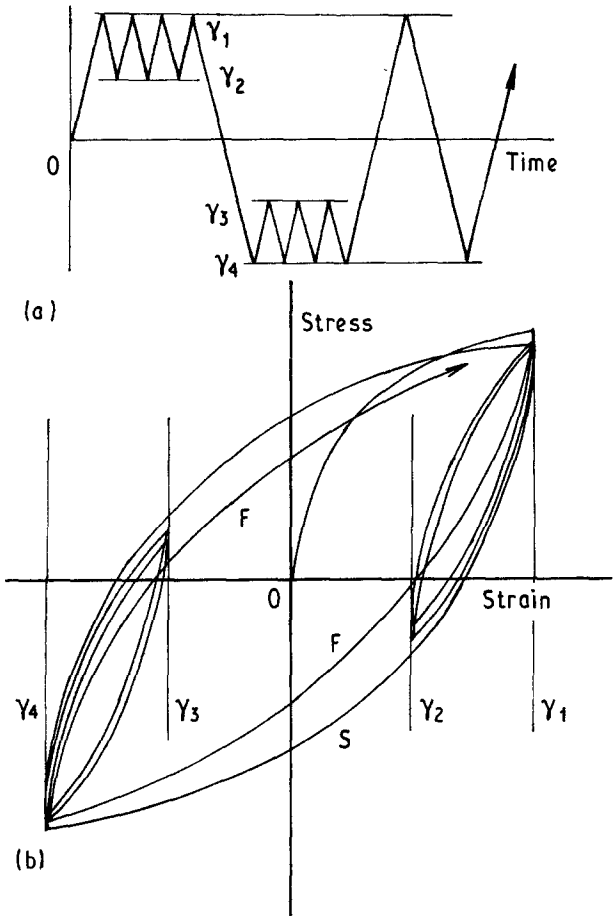

Figure 7 Schematic illustration for partly reversed cyclic loading: (a) waveform and (b) stress–strain behaviour.

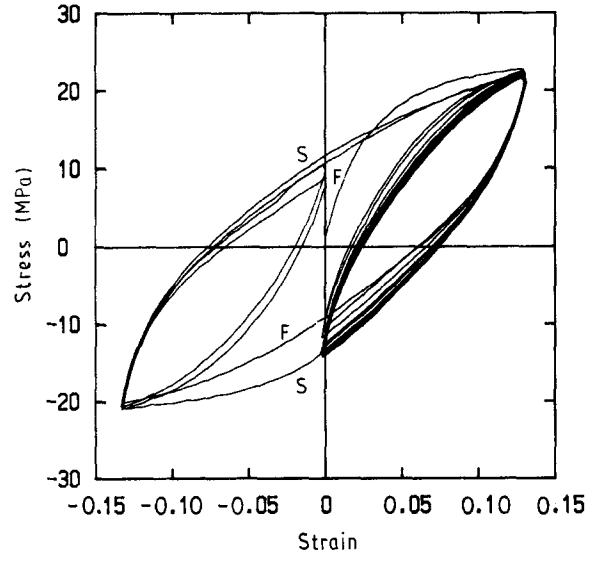

Figure 8 Torsional hysteresis loops for partly reversed cyclic loading with a triangular waveform at a strain rate of $1.8 \times 10^{-3} s^{-1}$ under hydrostatic pressure 1000 kgf cm^{-2}.

cyclic hardening appears to occur. This seems to contradict the case for fully reversed loading where the degree of cyclic softening is very small.

The effect of strain amplitude on the degree of cyclic softening was also measured, the maximum strain γ_1 being kept constant ($\gamma_{max.}$) and the minimum strain γ_2 being altered. Fig. 9 shows the hysteresis loops for different values of γ_2. It is found that (i) when

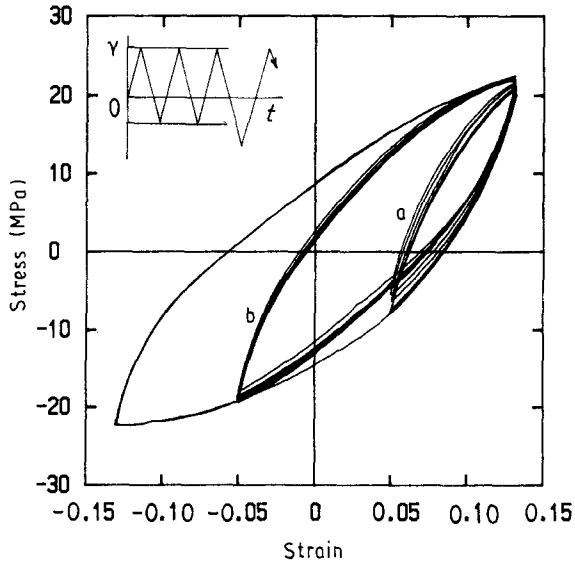

Figure 9 Torsional hysteresis loops at different strain amplitude for partly reversed cyclic loading with a triangular waveform at a strain rate of $1.8 \times 10^{-3} s^{-1}$ under hydrostatic pressure 1000 kgf cm^{-2}. Two loops (a) and (b) were obtained in different tests.

$\gamma_2 > -\gamma_{max.}$, cyclic hardening is clearly observed and (ii) its degree is dependent on γ_2. In general, the degree of cyclic hardening appears to be a maximum at about $\gamma_2 = 0$. As the strain $\gamma_{min.}$ increases (γ_1 becomes zero), the degree of cyclic hardening tends to become large.

After Step I, torsion was applied at the same strain rate from $\gamma = \gamma_{max.}$ to $\gamma = -\gamma_{max.}$. On the way to Step II, the curve marked S expands outwards and is situated outside the other curves. At Step II, results similar to those at Step I are observed. Therefore, the hysteresis loops at Step II become nearly symmetric with those at Step I with respect to the origin, and the material behaves as if it forgets the past strain paths.

At the final step (Step III), a fully reversed cyclic test was performed in the strain range $-\gamma_{max.}$ to $\gamma_{max.}$ in one cycle. The final loop F (situated inside the curve S) again reduces to the one obtained at the corresponding strain amplitude (the large loop in Fig. 10). This may indicate that the strain history plays no important role in the current stress–strain behaviour.

As mentioned above, the stress–strain behaviour seems to be not much affected by the strain history. In order to reconfirm this trend, an increasing and decreasing strain amplitude test was carried out. The strain path is schematically illustrated in Fig. 10. At each strain amplitude, several cycles are repeated. The current loop in a descending amplitude test nearly traces over the previous ones obtained at the same strain amplitude. This fact that the history dependence is very small for PE seems to be in a marked contrast to that for PP [20].

Further tests were carried out to investigate the effect of the strain history on the stress–strain behaviour. After cyclic torsional loading was applied for several cycles, the specimen was returned to an undeformed (zero strain) state and was left for about 2 h, which is required for sufficient stress relaxation to the state in which it was set on the testing machine. Consequently the residual torsional stress became

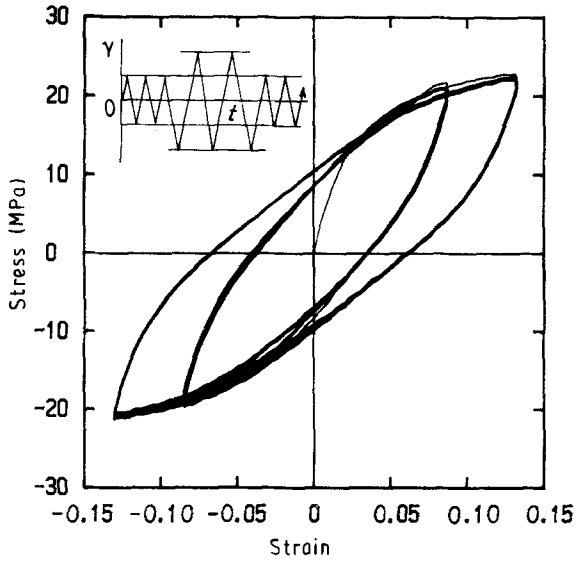

Figure 10 Hysteresis loops for increasing and decreasing strain amplitude with a triangular waveform at a strain rate of 1.8 $\times 10^{-3} s^{-1}$ under hydrostatic pressure 1000 kgf cm^{-2}. The strain amplitude changes between 0.085 and 0.13 as follows; 0.085 → 0.13 → 0.085 → 0.13.

nearly equal to zero. After this, the tension test was executed at the same equivalent strain rate as in the prior cyclic torsion. The stress–strain curves obtained are shown in a $\sigma_{eq.}$–$\varepsilon_{eq.}$ plot in Fig. 11, where the dotted curve corresponds to the tensile behaviour. The tensile stress–strain curve is almost coincident with the initial torsional one before the first strain reversal. This shows that cyclic torsion does not affect the later tensile behaviour. A test where the order of tension and torsion was reversed was also executed. A similar result was obtained. This may be very different from the case of metals. For metals, since the difference of the direction of dislocation motion between tension and torsion causes additional work-hardening in an anomalous fashion more strongly than expected, the latter curve becomes higher than the former one. This is called cross-hardening.

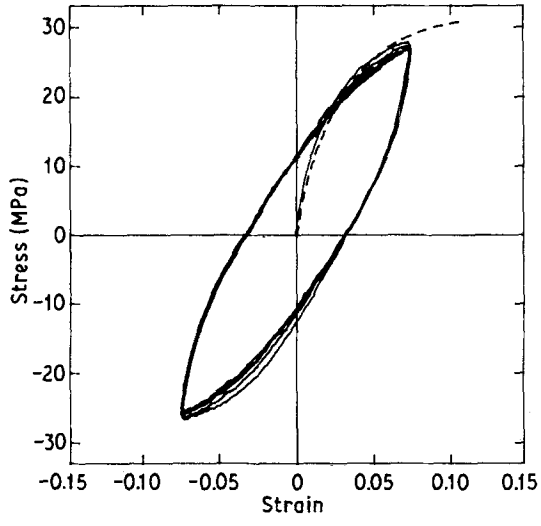

Figure 11 Tensile stress–strain curve (dotted curve) obtained after cyclic torsional loading (solid loops) in an equivalent stress–equivalent strain space. The cyclic torsion and monotonous tension were applied at an equivalent strain rate of $1.4 \times 10^{-3} s^{-1}$.

The above-mentioned results indicate that the stress–strain response for PE is insensitive to the strain history.

3.4. Special strain paths

The stress–strain responses were measured for more complex strain paths. The path shapes should be referred to the schematic illustrations shown in Table I.

The stress–strain behaviour was first investigated for a cyclic proportional strain path at a strain rate ratio of $3^{1/2}\ \varepsilon_n/\gamma = 1$ (see Table Ib). The principal direction of deformation does not change during this test and is kept constant. The waveform of applied strain for both tension and torsion is triangular. The applied strain path in a $\gamma/3^{1/2}$–ε plane and the experimental stress trajectory in a $3^{1/2}\tau$–σ plane are shown in Fig. 12a and b, respectively. Although the practical strain is controlled well to move along an expected

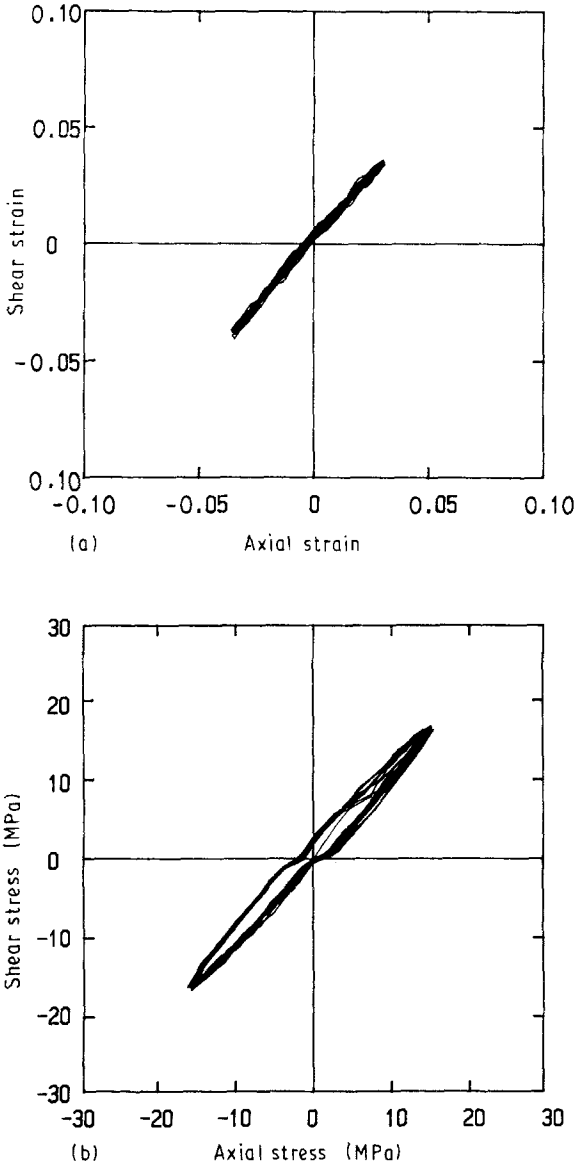

Figure 12 Stress–strain behaviour for proportional strain path (Table Ib) at an equivalent strain amplitude of 0.05. The strain rates are $\dot{\varepsilon} = \dot{\gamma}/3^{1/2} = 1.04 \times 10^{-3} s^{-1}$. (a) Practical strain trajectory in an equivalent strain plane and (b) stress trajectory in an equivalent stress plane.

linear path in every cycle, the stress trajectory consists of several narrow loops. However, the trajectory may be regarded as moving between the maximum and minimum points along a straight line denoted by $3^{1/2}\tau/\sigma = 1$ and seems to be independent of the number of cycles. Cyclic hardening is rarely observed in this case as well as in uniaxial loading. If the stress–strain curves are arranged in a $\sigma_{eq.}$–$\varepsilon_{eq.}$ diagram, hysteresis curves for both tension–compression and torsion are nearly coincident.

A partly reversed cyclic loading at a proportional strain path was also executed. The result was similar to that for the partly reversed cyclic torsion.

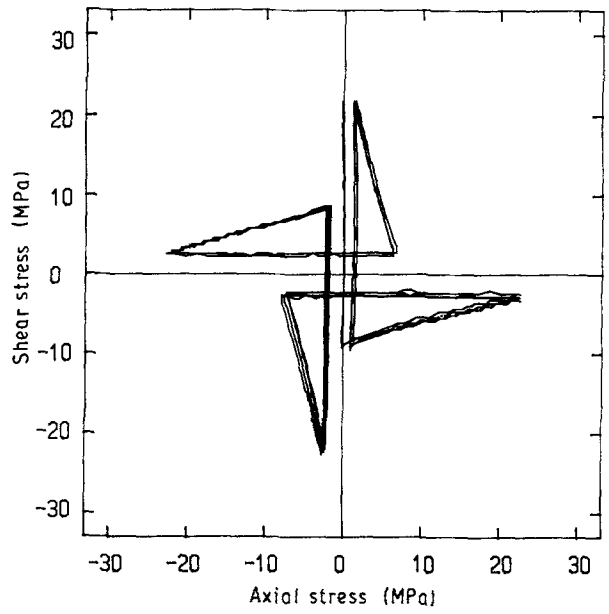

Figure 13 Stress trajectory for cyclic cruciform strain path with an equivalent strain amplitude of $\Delta\varepsilon_{eq.} = 0.05$ (Table Ic). The equivalent strain rate is $1.4 \times 10^{-3}\,s^{-1}$.

We next consider the stress–strain behaviour for the cruciform strain path denoted in Table Ic. Since the axial load and the torque act alternately, and therefore the principal direction of deformation changes for every loading process, this strain path may be convenient for investigating the strain path dependence. The result is shown in Fig. 13. In a $3^{1/2}\tau$–σ diagram, the stress trajectory is shaped as if four sails of a yacht are symmetrically placed with respect to the origin. This is very different from the shape for steels which is nearly circular in each quadrant. The trajectory seems independent of the number of cycles. This fact, that the stress–strain behaviour for PE is strain history-independent, supports the previous conclusion in Section 3.3.

Finally, let us consider the stress–strain behaviour for a cyclic circular strain path. Uniaxial tension or pure torsion was applied with a sinusoidal waveform until the circular strain path started. For the circular strain path, the axial strain ε and torsional strain γ and the equivalent strain rate $\varepsilon_{eq.}$ are written

$$\varepsilon = a\sin(\omega t)$$
$$\gamma = 3^{1/2} a\cos(\omega t) \quad (8)$$

$$\dot{\varepsilon}_{eq.} = a\omega \quad (9)$$

where a is the strain amplitude, ω the angular velocity and t the time. $a = 0.05$ and $\omega = 2.1 \times 10^{-2}$ rad s^{-1} and hence $\dot{\varepsilon}_{eq.} = 1.5 \times 10^{-3}\,s^{-1}$ were chosen. In the present test, the nominal axial strain and the nominal shear strain were controlled through a microcomputer. Since the equivalent strain amplitude is relatively small, the true axial strain rate $\dot{\varepsilon}$ may be estimated to be nearly equal to the nominal strain rate $\dot{\varepsilon}_n$. The results are shown in Fig. 14 where a test starts at

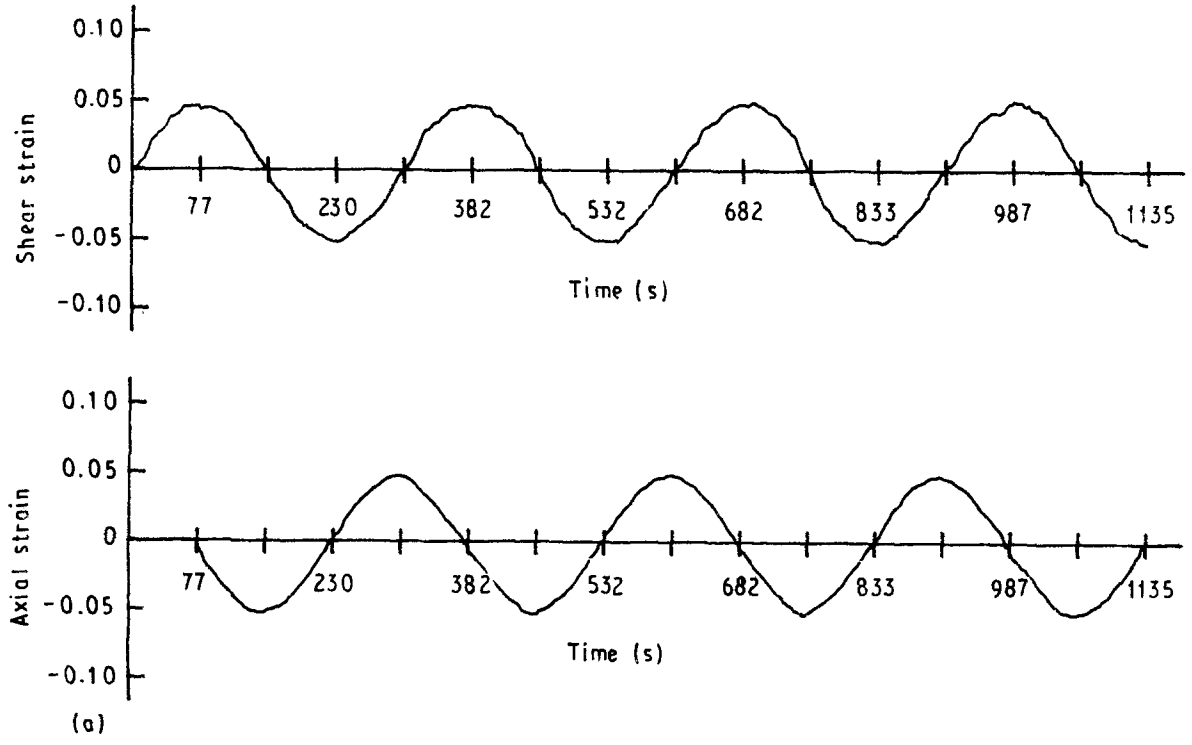

Figure 14 Stress–strain behaviour for cyclic circular strain path with an equivalent strain amplitude of $\Delta\varepsilon_{eq.}(= a) = 0.05$ (Table Id) at a cyclic frequency of 1/300 Hz. (a) Strain–time, (b) strain trajectory in a shear strain–axial strain plane, (c) stress–time and (d) stress trajectory in a shear stress–axial stress plane.

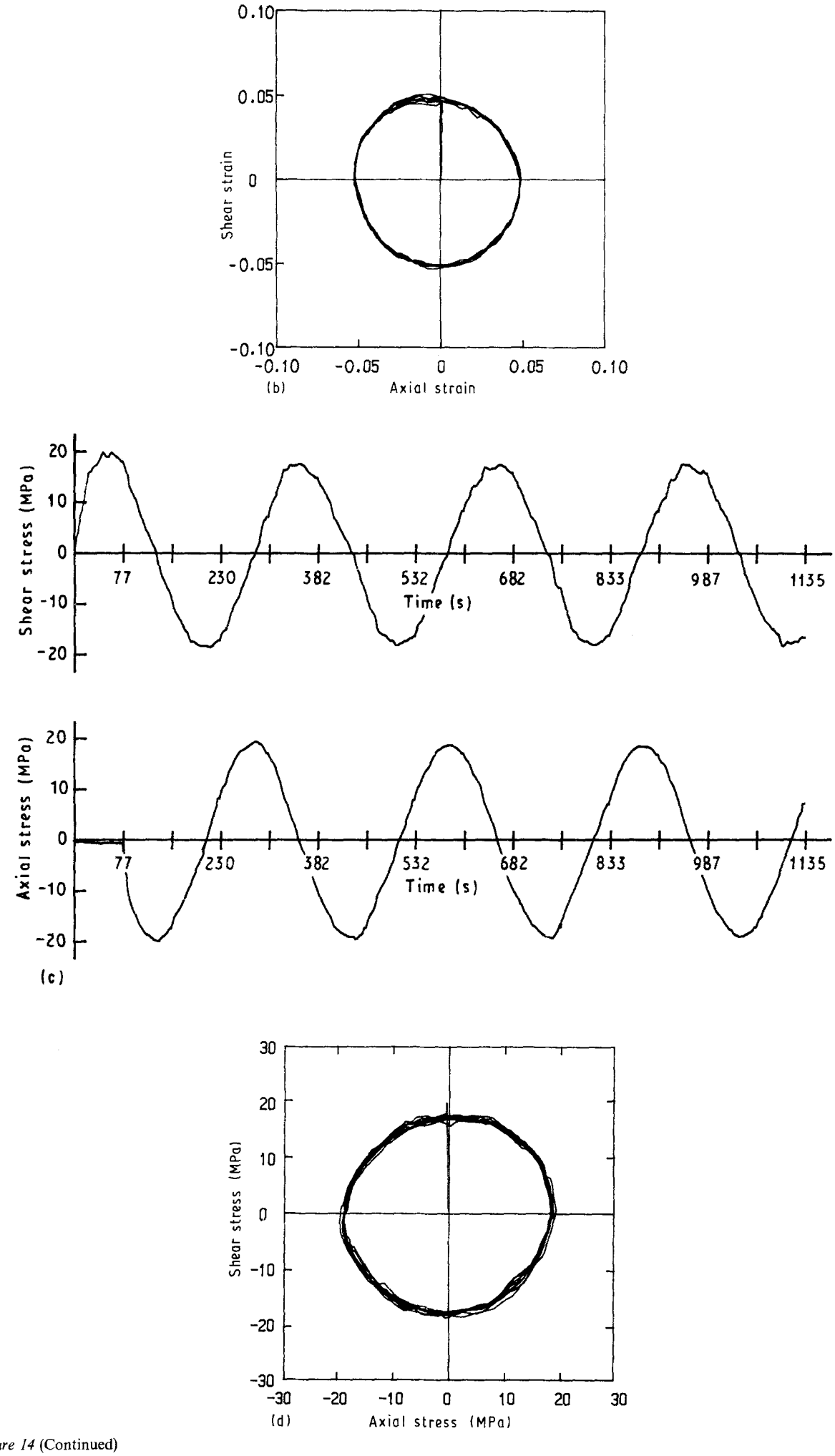

Figure 14 (Continued)

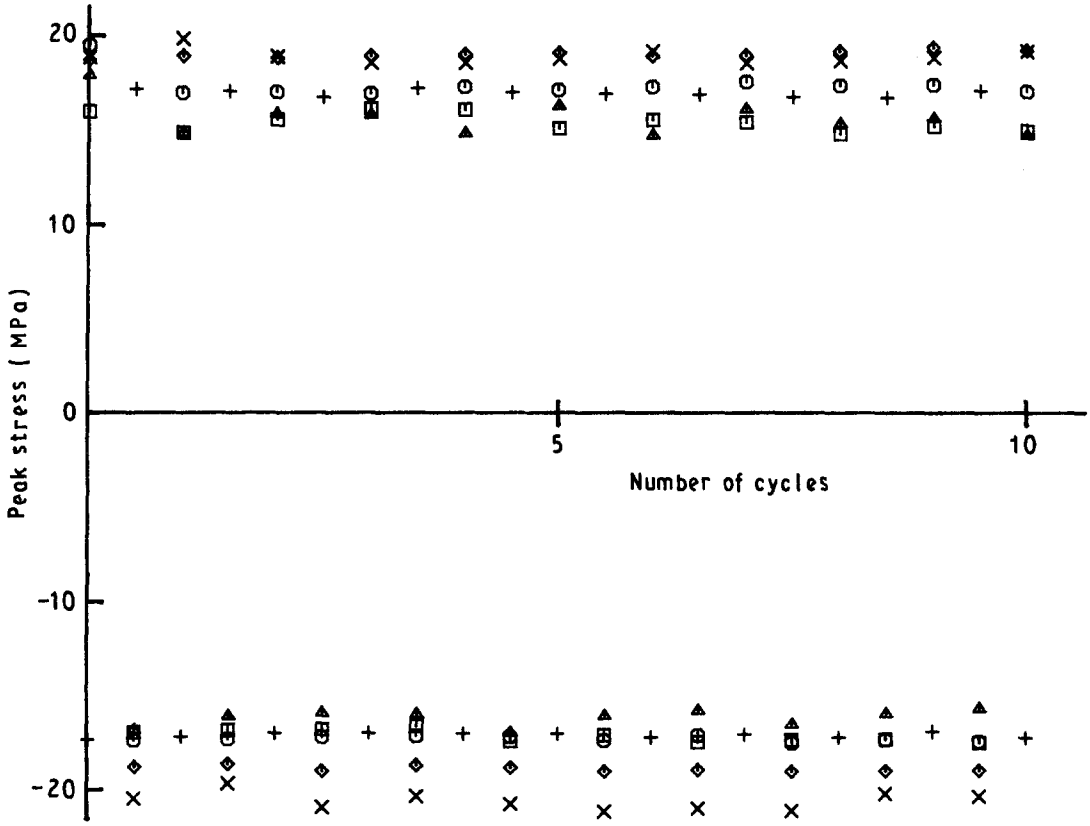

Figure 15 Variation of peak stress with an increase in cyclic number at an equivalent strain amplitude of 0.05 for (◇) tension–compression, (×) torsion, and circular strain paths: (○, □) tension prior to circular path, (+, Δ) torsion prior to circular path. Shear stress is converted to the equivalent tensile stress.

torsion. Fig. 14a, b, c and d show the actual strain path, the practical strain trajectory in a $\gamma/3^{1/2}$–ε plane, the stress response as a function of elapsed time and the stress trajectory in a $3^{1/2}\tau$–σ plane, respectively. In the case where uniaxial tension was applied preceding the circular path, similar results were also observed. As denoted in Fig. 14b, when the peak tensile stress is reached, the torsional stress is not always equal to zero, because of the phase lag between strain and stress. The converse is true. Hence the stress trajectory will somewhat depart from an exact circle, but since this departure is very small, the trajectory nearly becomes a circle independent of the number of cycles. The current trajectory appears to trace over the previous one.

Fig. 15 shows the variation of the torsional stress crossing the vertical axis and the axial stress crossing the horizontal axis with the number of cycles. The stresses are converted into the equivalent stress defined by Equation 7. The data for a test where tension was applied prior to the circular path, and the results denoted in Fig. 6, are also represented in the figure. The stresses for the circular paths are somewhat lower than in the uniaxial data. This is probably due to the fact that maximum stresses are not adopted for the circular strain path. It is clear that a significant cyclic softening or hardening is not observed, irrespective of the various strain paths adopted here. If the deformation mechanism of PE was mainly governed by a series of slip systems due to dislocation motion, the degree of cyclic hardening would be expected to be larger than this result due to the cross-hardening effect, since the slip direction changes during every cycle. Hence, the deformation behaviour is supposed to be very different from that of metals.

4. Conclusions

In order to investigate the constitutive equation for a crystalline polymer of polyethylene (PE), the stress–strain behaviour was observed for various strain paths such as uniaxial tension, torsion, combined tension–torsion and cyclic loading in a strain-controlled test. The PE material used here showed some strange stress–strain responses in that (i) the data arrangement by use of an equivalent stress and equivalent strain of von Mises type is appropriate, since PE is pressure-insensitive, and (ii) cyclic softening or hardening is hardly observed and hence the stress–strain behaviour is little affected by the strain history. This behaviour may be special in comparison with other crystalline polymers such as polypropylene and polyoxymethylene. In other words, since the stress–strain behaviour for PE is not so affected by the strain history and therefore is relatively simple, PE may be a useful material for the first step in considering a constitutive model for polymer solids.

References

1. I. M. WARD, *J. Mater. Sci.* **6** (1971) 1397.
2. R. M. CHRISTENSEN, "Theory of Viscoelasticity", (Academic, New York, 1971).

3. C. BAUWENS-CROWET, J. C. BAUWENS and G. HOMES, *J. Mater. Sci.* **7** (1972) 176.
4. P. B. BOWDEN and J. A. JUKES, *ibid.* **7** (1972) 52.
5. N. BROWN and I. M. WARD, *Phil. Mag.* **18** (1968) 483.
6. D. RABINOWITZ, I. M. WARD and J. S. C. PARRY, *J. Mater. Sci.* **5** (1970) 129.
7. C. BAUWENS-CROWET, J. C. BAUWENS and G. HOMES, *ibid.* **8** (1973) 176.
8. R. E. ROBERTSON, *J. Chem. Phys.* **44** (1966) 3950.
9. A. S. ARGON, *Phil. Mag.* **28** (1973) 839.
10. P. B. BOWDEN and S. RAHA, *ibid.* **29** (1974) 149.
11. D. M. PARKS and M. C. BOYCE, in "Constitutive Modeling for Nontraditional Materials", edited by V. Stokes and D. Krajcinovic, ASME, AMD, New York, Vol. 85 (1987) p. 1.
12. T. A. VEST, J. AMOEDO and D. LEE, *ibid.* p. 71.
13. M. KITAGAWA and T. MATSUTANI, *J. Mater. Sci.* **23** (1988) 4085.
14. M. KITAGAWA, T. MORI and T. MATSUTANI, *J. Polym. Sci. B* **27** (1989) 85.
15. M. KITAGAWA and H. TAKAGI, *J. Mater. Sci.* **25** (1990) 2869.
16. M. KITAGAWA and T. MATSUTANI, *J. Soc. Mater. Sci. Jpn* **37** (1988) 29.
17. E. KREMPL, *Trans. ASME, J. Appl. Mech.* **18** (1979) 380.
18. M. C. LIU and E. KREMPL, *J. Mech. Phys. Solids* **27** (1979) 377.
19. M. KITAGAWA and T. YONEYAMA, *J. Polymer Sci. C* **26** (1988) 207.
20. M. KITAGAWA, T. YONEYAMA, J. QUI and K. NISHIDA, *Jpn. Soc. Mech. Eng.* **A-57** (1991) 1680.

Received 19 October 1990
and accepted 25 March 1991